IEEE Access
Multidisciplinary | Rapid Review | Open Access Journal

Received May 7, 2018, accepted June 20, 2018, date of publication July 25, 2018, date of current version August 20, 2018.

Digital Object Identifier 10.1109/ACCESS.2018.2859840

Design and Implementation of a Two-Wheel and Hopping Robot With a Linkage Mechanism

YANHENG ZHANG[1], (Member, IEEE), LUFENG ZHANG[1], WEI WANG[2], YANGMIN LI[3], (Senior Member, IEEE), AND QINGWEN ZHANG[1]

[1]Automation School, Beijing University of Posts and Telecommunications, Beijing 100876, China
[2]School of Mechanical Engineering and Automation, Beijing University of Aeronautics and Astronautics, Beijing 100191, China
[3]Department of Industrial and Systems Engineering, The Hong Kong Polytechnic University, Hong Kong

Corresponding author: Yanheng Zhang (zyh620@bupt.edu.cn)

This work was supported by the Fundamental Research Funds for the Central Universities under Grant 2018PTB-00-10.

ABSTRACT Wheeled robots exhibit fast and stable motion on a flat road but lack the ability to overcome the obstacles and rough terrains. To address this shortage, a two-wheel hopping robot is proposed by combining the wheel locomotion and bounce movement. A gear train and a four-bar linkage are employed for jumping. In particular, the take-off angle is dependent on the link length of the four-bar linkage, thus providing versatile flight trajectories. Therefore, the dependency of the hopping performance on the four-bar linkage can be maximized. A four-bar linkage with the same length is used for the specific trajectory and balance control of the inverted pendulum model of the prototype. Dynamics analyses and simulations have been conducted to verify the robot design and its parameters. By jumping tests, the hopping performance is compared with other robots in a quantitative manner. The experimental results show that the wheeled hopping robot has the advantages of light mass and jumping height efficiency.

INDEX TERMS Two-wheel and hopping robot, four-bar linkage, motion analysis, hopping.

I. INTRODUCTION

It is well known that wheeled robots can move fast and are stable on a flat road, thus gaining high efficiency and low motion noise. In many cases, mobile robots are used for monitor, search and rescue (MSR). However, when wheeled robots are moving in uneven terrains, such as slopes and gullies, their intrinsic shortcomings appear. For example, they cannot overcome an obstacle when the radius of the wheel is less than the height of the obstacle or the contact point is above the center of the wheel. Because of the limitations on size and mass, a wheel diameter cannot be arbitrarily large. To date, how to improve their overcoming obstacle abilities is still a challenging problem.

To address this problem, many researchers implemented a number of wheeled climbing robots, such as the Whegs robot, which can climb obstacles 175% of its wheel radius due to a cockroach-like nominal tripod gait [1], and IMPASS, which can walk on various terrains, cross over obstacles, and climb up steps by intelligently extending and retracting its spokes [2]. When robots are moving in the uneven terrains, legged locomotion is an ideal alternative to wheels since it allows the use of isolated footholds, the ability to step over obstacles, and the ability to decouple the path of the body from that of the leg [3]. For instance, the self-adaptive robotic leg can passively change its transmission and shape to cross several big obstacles [4]. However, a legged or wheeled robot is not an effective solution to the problem of overcoming high obstacles.

Inspired by biological creatures, jumping is then regarded as not only an add-on to traditional wheeled robots but also an evolution in legged robots. Similar to what occurs in the natural world, jumping is an efficient method that helps robots overcome obstacles much higher than themselves [5], and even jump over an obstacle or gully several ten times of their own sizes. Therefore, compared with other locomotion modes, jumping shows good dynamic accelerating performance [6]. The jumping trajectory consists of a series of discrete take-off and landing points with a good adaptability to the ground. However, these robots can rarely realize fast traveling, economic jumping, posture control, and soft landing [7].

The typical wheel-legged robot "Handle" is designed for mobile manipulation and can jump 1.2 m high by employing hydraulic driven legs, but its large volume of nearly 1.98 m in height limits its applications [8]. Some other legged platforms such as HyQ [9], the Raibert hopper [10] and the MIT robot Cheetah [11] use a similar driving system. In contrast, "Salto" is less than 20 cm high and weighs only

100 grams and is designed to enhance power modulation, as well as minimize the mass and volume. Inspired by galagos, "Salto" is built using a series-elastic actuation (SEA) with a novel eight-bar revolute mechanism corresponding to an MA (mechanical advantage) profile. An MA is defined as the ratio of the reaction force at the foot to the force applied by the actuator. The average jumping height of this SEA+MA robot is 1.21 m±0.065 m, nearly 78% of the vertical jumping ability of a galago (the previous robots can reach 55% at most), which proves an efficient jumping design and strategy [12], [13]. Furthermore, "Salto-1P" is created for continuously hopping on the ground. Aerodynamic thrusters and an inertial tail are added to control its attitude in the air. "Salto-1P" can perform a standing vertical leap of 1.25 m, continuously hop to heights over 1 m, and jump over 2 m horizontally [14]. The mechanisms adopted by other jumping robots are presented in Table 1. A number of catch mechanisms are used in these small jumping robots. However, among these jumping robots, none of them provides the advantages of wheel motion.

TABLE 1. Energy charge and release mechanism of robots.

Name	Energy Charge and Release Mechanism
Miniature 7 g jumping robot[15]	Cam
Kangarobo[16]	Cam
Flea-like jumping robot[17]	Cam
Surveillance robot[18]	Winch mechanism with an incomplete gear
Integrated jumping-crawling robot[19]	Active triggering mechanism with a planet gear
SandFlea[20]	Disposable fuel
Single-leg robot[21]	Eccentric slider crank
TAUB[22]	Latch mechanism
Wheeled hopping robot	Gear train with two incomplete gears

The robot proposed in this paper is 132×54×168 mm in size. Both the wheel mode and jumping mode are involved in this small-sized robot. Not only can the robot move stably and quickly using the wheels but also the jumping trajectory, such as the take-off angle and balance control, can all be justified through the wheels. This paper is organized as follows: In Section 2, the principle of the wheeled-hopping robot is provided, including the gear train for energy charge and release, and the four-bar linkage with a torsional spring used to act as the jumping actuator. The jumping dynamics model is built and analyzed in Section 3. In Section 4, the simulation is conducted to optimize the structure of the robot. The prototype is fabricated, and experiment results are shown in Section 5 to verify and assess the robot design. The paper is concluded in the last section.

II. DESIGN PRINCIPLE

It is obvious that the mass distribution of the robot should be designed in an optimal fashion so that the jumping height and jumping distance could be maximized. The mass distribution between the legs and the main body of the robot is governed by (1).

$$\tau = \frac{E}{m_u d} = \frac{E}{m_u \frac{v_0^2 \sin 2\alpha_0}{g}} = \frac{g}{2\,(1-\lambda)\sin(2\alpha_0)} \tag{1}$$

where λ is the mass ratio of the leg to the robot, α_0 is the take-off angle and the "cost of transport" τ is defined as the kinetic energy of a jumping system divided by the mass and distance of a jump. It can be an indicator for the jumping efficiency. Therefore, the cost function τ is inversely proportional to the mass ratio λ [23]. To obtain high jumping efficiency, the weight of the legs should be reduced and most of the mass, such as the gear train and control panel, should be placed close to the top of the body. The actuator of the robot will be discussed later. The robot's trajectory of overcoming obstacles is shown in Figure 1.

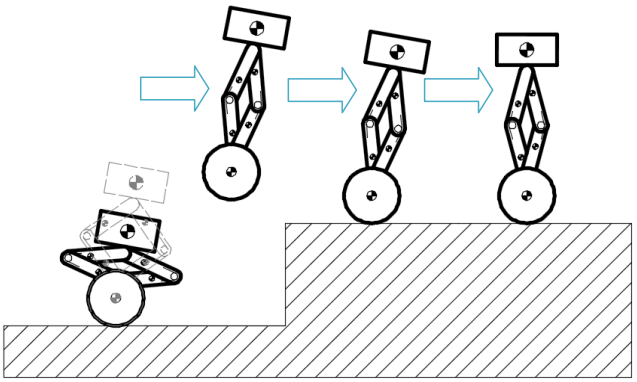

FIGURE 1. Trajectory of overcoming obstacles.

A. ENERGY CHARGE AND RELEASE MECHANISM

One of the most important features in hopping robots is the energy charge and release mechanism with the characteristic of quick-return motion. Thus, the energy charge and release mechanism can release the stored elastic energy in very short time to ensure a sufficiently great reaction force between the ground and the robot foot. Because of the sufficient reaction, the initial velocity and the initial acceleration at the moment of jumping can be triggered. The commonly used bounce triggering mechanism is summarized in Table 1.

A gear system with two incomplete gears is employed in our hopping robot, providing the benefit of saving space compared to a cam. The gear train consists of an active gear, two transmission gears and two pulley gears, as shown in Fig. 2. When the active gear is driven counter-clockwise by the motor, the cable passing around the pulley will be tightened in a slow manner until the incomplete gears and pulley gears disengage from each other because of the missing teeth. Immediately after that, the pulley gear is released, and the jumping mode begins.

B. PARALLEL LINKAGE FOR HOPPING

The main advantage of a four-bar linkage is that the trajectory of a link can be modified by changing the length of the bars. When it is used for the leg design, the take-off angle could

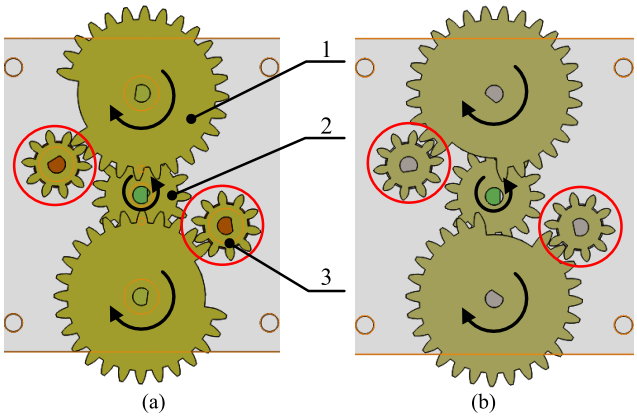

FIGURE 2. Gear train for energy charge and release: 1-Transmission gear 2-Active gear 3-Pulley gear. (a) Pulley gear starts winding; (b) Pulley gear starts releasing the cable.

be modified, and the ground reaction force profile could be improved [24]. The design of the four-bar linkage is to solve the ideal trajectory of jumping. For instance, to achieve high jumping and fast running, the leg in the Kangaroo-inspired robot has four bars with different lengths to resemble a real Kangaroo leg, where the horizontal length is greater than the vertical length [16]. The leg inspired by the musculoskeletal structure in the robot leg involved high performance and dynamic efficiently locomotion, including walking, running and especially jumping in the vertical direction, which was realized by a parallel linkage [24].

The ideal jumping trajectory of the robot in this paper is shown in Figure 3. To balance the robot, the four-bar linkage should be arranged in a right-left symmetry with one torsional spring on each joint of the front and the back joints. The main reason for the use of the torsional springs here is that they are more space-saving than linear springs.

III. DYNAMICS MODEL

As the wheel and hopping robot is in a right-left symmetry form, it can be simplified to a 2D model in the X-Y plane, as shown in Figure 4. When facing an obstacle, the robot is designed to overcome the obstacle in the way shown in Figure 1. During the take-off phase, a coordinate system is attached to the contact point between the wheel and the ground, the four bars are indexed counter-clockwise as in Figure 4. Additionally, α is the inclination angle of the body relative to the Y-axis.

The kinetic energy for jumping is gained from the elastic potential energy of the torsional spring and is generated through the reaction force with the ground F_x, F_y.

$$F_x = \sum_{i=1}^{4} m_i \ddot{x}_i + m_w \ddot{x}_w + m_u \ddot{x}_u \tag{2}$$

$$F_y = \sum_{i=1}^{4} m_i \ddot{y}_i + m_w \ddot{y}_w + m_u \ddot{y}_u - \left(\sum_{i=1}^{4} m_i g + m_w g + m_u g \right) \tag{3}$$

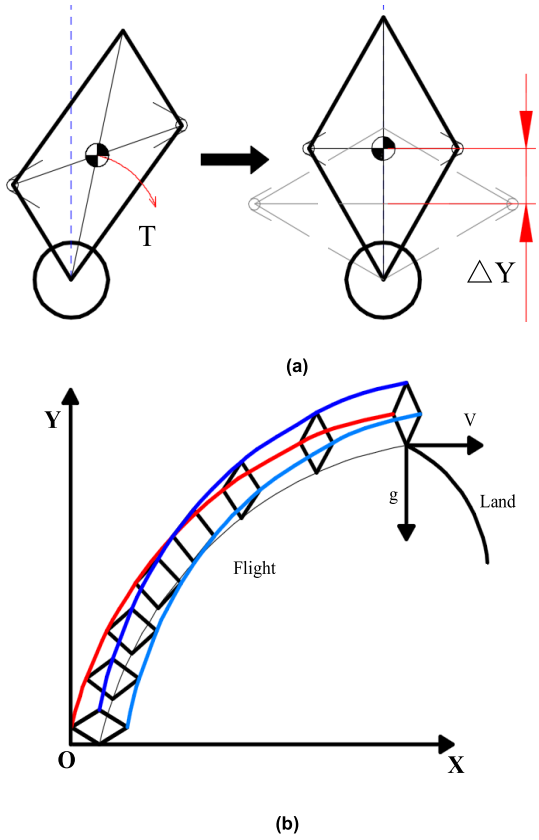

FIGURE 3. Parallel linkage for hopping: (a) Four-bar linkage optimization based on T and ΔY; (b) Ideal trajectory of jumping.

In equations (2) and (3), m_i $(i = 1, 2, 3, 4)$ is the mass of each part of the robot, m_w is the combined mass of the wheel and the motor and m_u is the mass of the upper body. The position of the parts is given by:

$$\begin{cases} x_w = 0 \\ x_1 = h\tan\alpha + d\cos\left(\frac{\theta}{2} - \alpha\right) \\ x_2 = h\tan\alpha + L\cos\left(\frac{\theta}{2} - \alpha\right) - d\cos\left(\frac{\theta}{2} + \alpha\right) \\ x_3 = -d\cos\left(\frac{\theta}{2} - \alpha\right) + s\sin\alpha \\ x_4 = -b\sin\left(\frac{\theta}{2} - \alpha\right) + h\tan\alpha \\ x_u = (s + r + e)\sin\alpha \\ y_w = R \\ y_1 = R + h + d\sin\left(\frac{\theta}{2} - \alpha\right) \\ y_2 = h + R + L\sin\left(\frac{\theta}{2} - \alpha\right) + d\sin\left(\frac{\theta}{2} + \alpha\right) \\ y_3 = R + s\cos\alpha - d\sin\left(\frac{\theta}{2} - \alpha\right) \\ y_4 = R + h + b\cos\left(\frac{\theta}{2} - \alpha\right) \\ y_u = R + (s + r + e)\cos\alpha \end{cases} \tag{*}$$

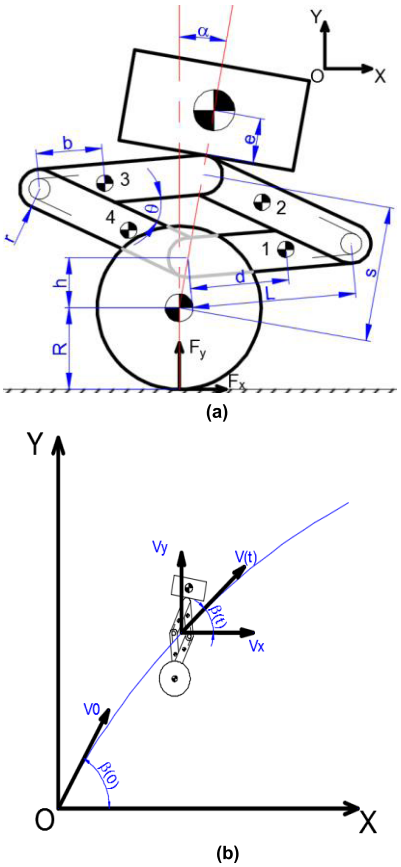

FIGURE 4. Force analysis in the take-off and flight phases. (a) Take-off state. (b) Flight state.

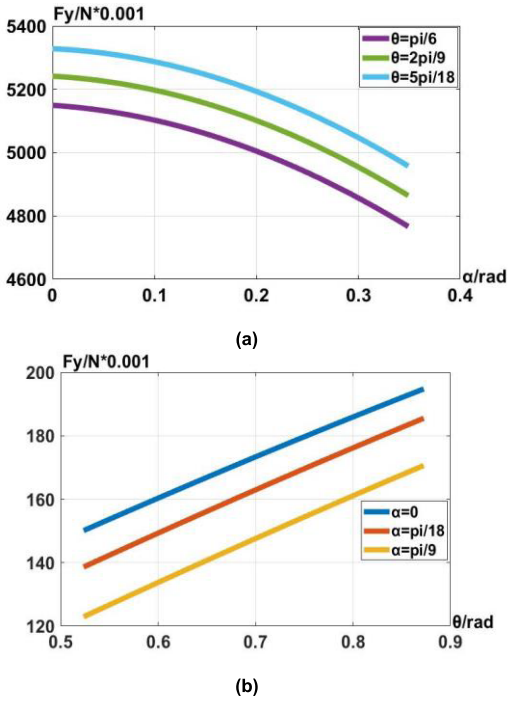

FIGURE 5. Relationship of F_y, α and θ.

Once the mass and length of the robot have been designed, the angles α and θ have a significant impact on the reaction force between the body and the ground. If the second-order derivation of the position coordinates is taken and m is substituted into equation (3), then the two variables that affect the reaction force and then the take-off acceleration can be determined. Based on the parameters in Table 2, the analysis results are shown in Fig. 5.

According to Fig. 5, it can be seen that F_y decreases with the increase of α, which indicates that the more inclined the body is to the ground, the smaller the take-off acceleration is. In contrast, F_y increases when θ increases, showing that it is necessary to use a torsional spring with a large pre-angle to obtain the desired take-off acceleration. However, the energy for hopping will decrease based on the following equation:

$$\frac{1}{2}mv_0^2 = \frac{1}{2}KN\left(\Delta\theta\right)^2 \tag{4}$$

K is the torsional stiffness coefficient, N is the number of springs and $\Delta\theta$ is the deflection angle of the springs. When the robot flies in the air, the air friction force is:

$$F_{air}\left(t\right) = \frac{1}{2}\rho v^2\left(t\right)Ac_d \tag{5}$$

Where ρ is the air density, $v\left(t\right)$ is the velocity of the robot, A is the frontal area and c_d is the drag coefficient. Thus, according to Figure 4 (b), the horizontal and vertical accelerations are:

$$a_x = -F_{air}\cos\left(\beta\left(t\right)\right)/m \tag{6}$$

$$a_y = \left(-F_{air}\sin\left(\beta\left(t\right)\right) - mg\right)/m \tag{7}$$

Then, we have

$$\dot{x}\left(t\right) = -\frac{1}{2m}\rho Ac_d\cos\left(\arctan\left(\frac{\dot{y}\left(t\right)}{\dot{x}\left(t\right)}\right)\right)\left(\dot{x}\left(t\right)^2 + \dot{y}\left(t\right)^2\right) \tag{8}$$

$$\dot{y}\left(t\right) = -\frac{1}{2m}\left[2g + \rho Ac_d\sin\left(\arctan\left(\frac{\dot{y}\left(t\right)}{\dot{x}\left(t\right)}\right)\right) \times\left(\dot{x}\left(t\right)^2 + \dot{y}\left(t\right)^2\right)\right] \tag{9}$$

The initial velocity of the robot v_0 is nearly 2 m/s based on equation (16), and if $\beta\left(0\right) = 80^0$ is assumed, then the initial conditions can be expressed as:

$$x\left(0\right) = 0 \tag{10}$$

$$y\left(0\right) = 0 \tag{11}$$

$$\dot{x}\left(0\right) = v_0\cos\left(\beta(0)\right) = 0.35m/s \tag{12}$$

$$\dot{y}\left(0\right) = v_0\sin\left(\beta(0)\right) = 1.97m/s \tag{13}$$

The numerical simulation is carried out based on equations (8) $\sim$ (13), and the analysis of the relationship between the velocity and the hopping time is shown in Fig. 6. The curve in Fig. 6(b) is a part of that in Fig. 6(a). The initial velocity of the robot is given directly from equations (12) $\sim$ (13), and the hopping process takes less than 40 ms when the vertical velocity is reduced to zero and the robot reaches the highest point. In addition, Fig. 6(a)

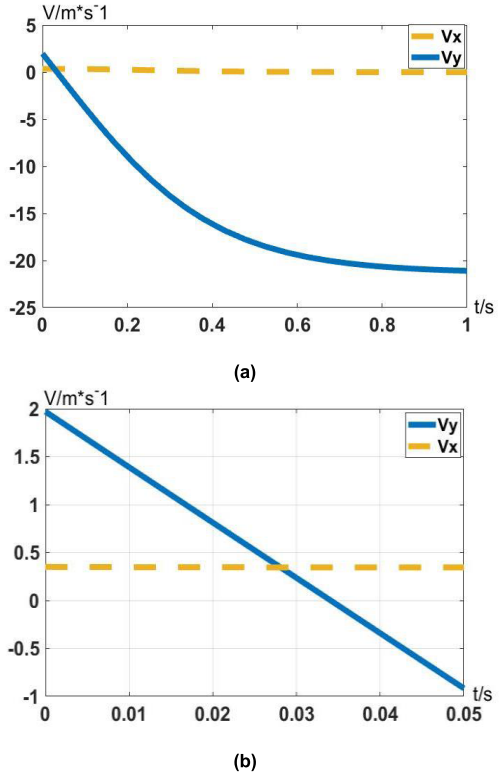

FIGURE 6. Velocity change during the jumping process.

shows that the deceleration process is changed in a nonlinear way, and the acceleration in the horizontal direction is much smaller than that in the vertical direction because of the gravity acceleration g.

TABLE 2. Parameters of the robot.

Parameters	Value	Unit
R	25	mm
L	50	mm
h	15.26	mm
s	41.38	mm
d	30	mm
r	6	mm
b	20	mm
e	14	mm
m_w	46	g
$m_i\,(i=1,2,3,4)$	7.5	g
m_u	64	g
Total Weight	170	g
ρ	1.3	Kg/m^3
A	0.075	m^2
C_d	1.3	const
$\Delta\theta$	120	degree

IV. SIMULATION

A virtual prototype is built to investigate the performance of the jumping robot, as shown in Fig. 7(a). The mass property is attached to each part according to Table 2. The velocity

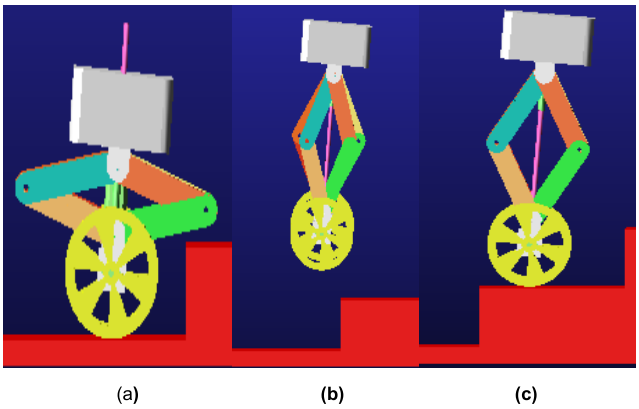

FIGURE 7. Simulation of the jumping process. (a) Initial state. (b) Non-equal speed. (c) Landing state.

and the reaction force of jumping are observed in the simulation. A number of situations in the software are likely to occur during an actual experiment, for example, the speeds of the two wheels are different from each other, as shown in Fig. 7(b). Thus, the reaction forces applied on each wheel are not equal, as shown in Fig. 8(b). The different states of the wheels are most likely to occur in reality and should be given particular attention. The simulated results are presented in Fig. 8 and Fig. 9.

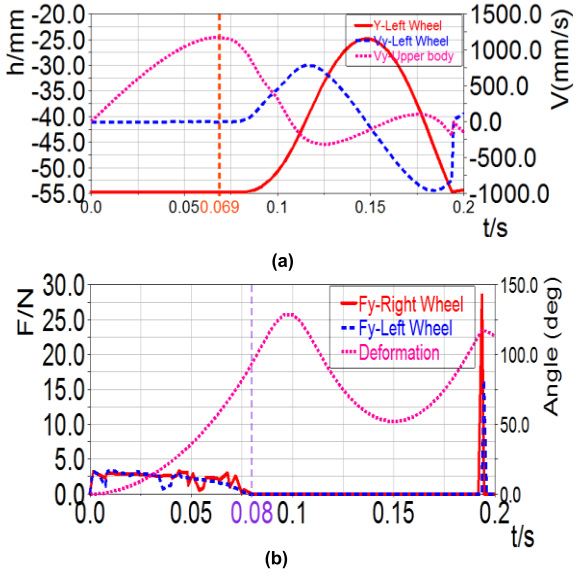

FIGURE 8. Simulation results of the robot. (a) Motion of the left wheel and upper body. (b) Reaction force of the wheels.

From Fig. 8(b), it can be seen that the interaction between the ground and the robot lasts 80 ms, and the opening angle of the torsional spring is 93.76 degrees, which is larger than the natural state of 90 degrees. It can be found that the torsional spring has been released to the natural state before the robot leaves the ground. In Fig. 8(a), we can see that the velocity of the upper body begins to decrease at 69 ms. At that moment, the wheel's velocity is still maintained at zero. This is because

the upper body needs be accelerated for a while first, and then the wheels are driven up in a way similar to an ''inelastic collision'' [36]. During this period, the torsional spring is released to a larger angle than the natural state. When the speed of the upper body is reduced to zero, the robot reaches the highest point similar to that shown in Fig. 6.

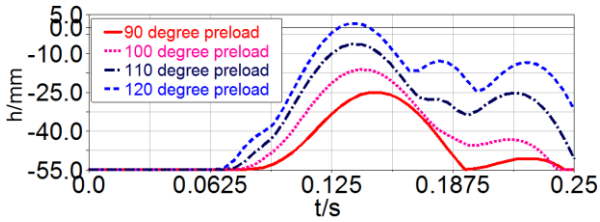

FIGURE 9. Motion state of the left wheel vs preload of the torsional spring.

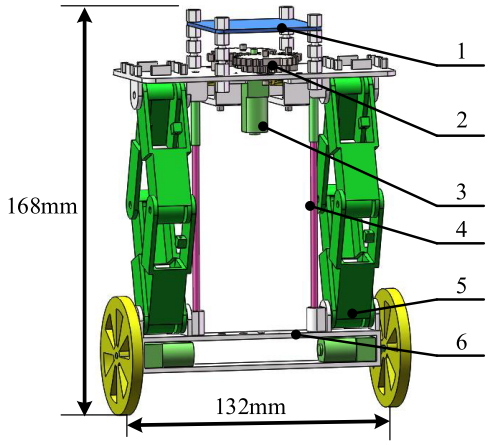

FIGURE 10. CAD model of the two-wheel and hopping robot: 1-Control panel 2-Gear train 3-DC motor 4-Guide bar 5-Four-bar linkage 6-Wheel frame.

Four torsional springs with different preloads but the same stiffnesses were used in the simulation, and the results are shown in Fig. 9, indicating that the larger the pre-angle is, the higher the robot can jump because more elastic energy is charged before jumping. Obvious second-bounces are generated by a torsional spring that is greatly preloaded. Due to the energy loss during jumping, especially for a collision in the landing phase, the height of the second bounce is much smaller than the height of the first jump.

By the simulation, it is possible that the two four-bar linkages are not in the same flight state, such as the time to take off, the pose in the air and the extent of the expansion at one moment. The main reason is that the release process of the torsional springs is not exactly the same. Therefore, the wheel frames on both sides should be rigidly connected for good balance control and stable landing. During a stable landing, the energy transfer should be maximized while landing. Therefore, the material of the wheel should be soft to a certain extent. The height difference between the second bounces is less than 10% according to Fig. 9; therefore, 120 degrees is selected as the preangle of the torsional spring in our experiments.

V. PROTOTYPE AND EXPERIMENTS

The two-wheel and hopping robot is designed, as shown in Fig. 10, with a control panel, a gear train, a guide bar, a four-bar linkage, and a wheel frame. Each wheel is driven by a DC motor, and the hopping mechanism is driven by another DC motor located on the upper part of the robot. The output torque of the motor is 0.196 N‧m. The guide bar is used to ensure that the four-bar linkage can be compressed and released in the vertical direction. The four-bar linkage can be deformed in the range from 110 mm to 40 mm for a potential jump.

The control method is introduced here. In the balanced upright phase, because of the gravity of the robot, the robot is likely to lose balance and fall. The angle between the robot and the vertical axis must be controlled in a specific range to keep the robot in a balanced state. Differing from the switched linear controller in [37], PID controller is adopted to balance the robot in this paper. The angle between the robot and the vertical axis is fed back to the controller, and a torque command is generated to drive the wheels to cause the robot to be in a vertical state. The control process can also be described in detail as follows: the value of the angular displacement sensor (MPU6050) is collected through STM32, and then the value of PWM is adjusted based on the PID control algorithm, so that the speed of the wheels can be changed. During this process, the value of PD is mainly adjusted. That means the value of Kp is gradually increased until there is a reverse or low frequency jitter and the differential control parameter Kd is used to control the trend of deviation, referring to suppressing the moment of inertia (ie, excessive rotation). Finally, the balance of the inverted pendulum model is achieved.

Screenshots are taken from the video of the jumping experiments, as shown in Fig. 11. The robot performed the jumping task successfully. The average jumping height is 120 mm, and the maximum height is 140 mm. The horizontal jumping distance is above 50 mm. The initial velocity is 1.66 m/s. Compared to the simulation results, the experimental results yield better jumping performance. The main reason is that a torsional spring with a larger stiffness coefficient is used in our experiments compared with that used in the simulation. A slight instability, such as a second bounce, occurred in both the experiments and simulation.

There are measures for assessing the jumping performance, such as the maximum jumping height. The ratio between the jumping heights to its own maximum size is another frequently used measure. Furthermore, the ability of continuous jumping is also important to the jumping robots, so the integrity of motion can be ensured. In the terms of these measures, the jumping performance of the abovementioned well-known jumping robots is evaluated in Table 3.

Many advantages can emerge from the combination of different motion modes. In this paper, both continuous jumping and stable movement can be achieved by the robot. It can be

TABLE 3. Comparision of the jumping robot.

Robot	Motion Mode		Continuous Jumping/Yes or Not	Mass/g	MS= Max. Size/cm	JH= Jumping Height/cm	$\frac{JH}{MS}$
	Jumping	Moving					
MiniWheg[32]	√	Unstable	Yes	190	15.5	18	1.16
Scout[35]	√	√	Yes	200	11	30	2.73
Grillo[20]	√	×	Yes	80	7	5	0.71
Salto-1P[14]	√	×	Yes	98.1	15	125	8.33
MultiMO-Bat[34]	√	×	Yes	115.6	30	305	10.17
SandFlea	√	√	Not	4990	unknown	800	-
Handle	√	√	Yes	unknown	198	120	0.61
Wheeled hopping robot	√	√	Yes	170	16.8	14	0.83

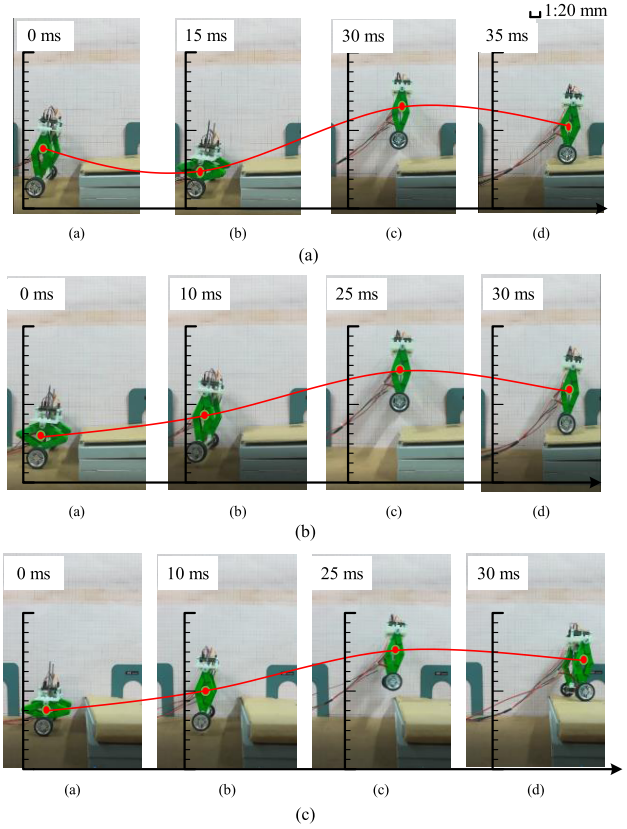

FIGURE 11. Snapshots of the moving and hopping experiments.

seen from Table 3 that among the jumping robots that can move stably and jump continuously, this wheeled hopping robot exhibits the lightest mass. In terms of the ratio of JH and MS, this robot shows better jumping performance than does Handle.

VI. CONCLUSION

In this article, a novel two-wheeled and hopping robot is proposed. The robot combines the wheel and hopping mechanisms and thus provides a new design idea for the MSR mission in a small-scale area. A four-bar linkage is employed in the robot to generate a hopping motion, and the stable movement of the robot on the road is obtained by wheels. The elastic energy is released by a specially designed gear train. The release process is simulated, and the simulated results indicate that the torsional spring is fully released at the time when the robot takes off. Taking advantage of the great deformation of the four-bar linkage, the minimum jumping height of the robot is greater than 117 mm. Compared to "Handle," which can jump up to 61% of its own height, our robot can jump up to 83% of its height, which is 14 cm. Moreover, the realization of continuous jumping is another highlight, which allows the robot overcome continuous obstacles on the road, thus ensuring the integrity of the entire motion driven by wheels. During the jumping process, the pose of the robot must be maintained in a stable range during landing. In our future work, to further improve the jumping height of the wheeled hopping robot, other bar linkages will be designed to increase energy efficiency. The second point is to optimize the control algorithm to obtain better robustness and balance performance while jumping and landing.

REFERENCES

[1] R. T. Schroer, M. J. Boggess, R. J. Bachmann, R. D. Quinn, and R. E. Ritzmann, "Comparing cockroach and Whegs robot body motions," in *Proc. IEEE Int. Conf. Robot. Automat. (ICRA)*, vol. 4, Apr./May 2004, pp. 3288–3293.

[2] J. B. Jeans and D. Hong, "IMPASS: Intelligent mobility platform with active spoke system," in *Proc. IEEE Int. Conf. Robot. Automat.*, May 2009, pp. 1605–1606.

[3] M. H. Raibert, "Legged robots," *Commun. ACM*, vol. 29, no. 6, pp. 499–514, 1986.

[4] D. Fedorov and L. Birglen, "Design of a self-adaptive robotic leg using a triggered compliant element," *IEEE Robot. Autom. Lett.*, vol. 2, no. 3, pp. 1444–1451, Jul. 2017.

[5] S. M. Song and K. J. Waldron, "Machines that walk: The adaptive suspension vehicle," NASA Sci. Tech. Inf., Tech. Rep., 1989, vol. 89, no. 6, pp. 7–12.

[6] F. Li *et al.*, "Jumping like an insect: Design and dynamic optimization of a jumping mini robot based on bio-mimetic inspiration," *Mechatronics*, vol. 22, no. 2, pp. 167–176, Mar. 2012.

[7] K. Kikuchi, K. Sakaguchi, T. Sudo, N. Bushida, Y. Chiba, and Y. Asai, "A study on a wheel-based stair-climbing robot with a hopping mechanism," *Mech. Syst. Signal Process.*, vol. 22, no. 6, pp. 1316–1326, 2008.

[8] *Boston Dynamics*. Accessed: Jul. 21, 2017. [Online]. Available: www.bostondynamics.com

[9] T. Boaventura, C. Semini, J. Buchli, M. Frigerio, M. Focchi, and D. G. Caldwell, "Dynamic torque control of a hydraulic quadruped robot" in *Proc. IEEE Int. Conf. Robot. Automat.*, May 2012, pp. 1889–1894.

[10] M. H. Raibert, H. B. Brown, Jr., and M. Chepponis, "Experiments in balance with a 3D one-legged hopping machine," *Int. J. Robot. Res.*, vol. 3, no. 2, pp. 75–92, 1984.

[11] D. J. Hyun, S. Seok, J. Lee, and S. Kim, "High speed trot-running: Implementation of a hierarchical controller using proprioceptive impedance control on the MIT Cheetah," *Int. J. Robot. Res.*, vol. 33, no. 11, pp. 1417–1445, 2015.

[12] D. W. Haldane, M. Plecnik, J. K. Yim, and R. S. Fearing, "A power modulating leg mechanism for monopedal hopping" in *Proc. IEEE/RSJ Int. Conf. Intell. Robots Syst.*, Oct. 2016, pp. 4757–4764.

[13] D. W. Haldane, M. M. Plecnik, J. K. Yim, and R. S. Fearing, "Robotic vertical jumping agility via series-elastic power modulation," *Sci. Robot.*, vol. 1, no. 1, p. eaag2048, 2016.

[14] D. W. Haldane, J. K. Yim, and R. S. Fearing, "Repetitive extreme-acceleration (14-g) spatial jumping with Salto-1P," in *Proc. IEEE/RSJ Int. Conf. Intell. Robots Syst.*, Sep. 2017, pp. 3345–3351.

[15] M. Kovac, M. Fuchs, A. Guignard, J.-C. Zufferey, and D. Floreano, "A miniature 7g jumping robot," in *Proc. IEEE Int. Conf. Robot. Automat.*, May 2008, pp. 373–378.

[16] B. R. Jun, Y. J. Kim, and S. Jung, "Design and control of jumping mechanism for a Kangaroo-inspired robot," in *Proc. IEEE Int. Conf. Biomed. Robot. Biomechatronics*, Jun. 2016, pp. 436–440.

[17] S. R. Buksh, X. Chen, and W. Wang, "Design and modeling of a flea-like jumping robot," in *Proc. IEEE Int. Conf. Control Automat.*, Dec. 2009, pp. 1862–1867.

[18] G. Song, K. Yin, Y. Zhou, and X. Cheng, "A surveillance robot with hopping capabilities for home security," *IEEE Trans. Consum. Electron.*, vol. 55, no. 4, pp. 2034–2039, Nov. 2009.

[19] G.-P. Jung, C. S. Casarez, S.-P. Jung, R. S. Fearing, and K.-J. Cho, "An integrated jumping-crawling robot using height-adjustable jumping module," in *Proc. IEEE Int. Conf. Robot. Automat.*, May 2016, pp. 4680–4685.

[20] U. Scarfogliero, C. Stefanini, and P. Dario, "The use of compliant joints and elastic energy storage in bio-inspired legged robots," *Mechanism Mach. Theory*, vol. 44, no. 3, pp. 580–590, 2009.

[21] D. Chang, J. Kim, D. Choi, K.-J. Cho, T. Seo, and J. Kim, "Design of a slider-crank leg mechanism for mobile hopping robotic platforms," *J. Mech. Sci. Technol.*, vol. 27, no. 1, pp. 207–214, 2013.

[22] V. Zaitsev, O. Gvirsman, U. B. Hanan, A. Weiss, A. Ayali, and G. Kosa, "Locust-inspired miniature jumping robot," in *Proc. IEEE/RSJ Int. Conf. Intell. Robots Syst.*, Sep./Oct. 2015, pp. 553–558.

[23] M. Kovac, *Bioinspired Jumping Locomotion for Miniature Robotics*, EPFL, Lausanne, Switzerland, 2010.

[24] A. Ming, K. Sato, R. Sato, E. Kazama, I. Miyamoto, and M. Shimojo, "Development of robot leg composed of parallel linkage and elastic spring for dynamic locomotion," in *Proc. IEEE Int. Conf. Inf. Automat.*, Aug. 2015, pp. 38–43.

[25] J.-S. Koh, S.-P. Jung, M. Noh, S.-W. Kim, and K.-J. Cho, "Flea inspired catapult mechanism with active energy storage and release for small scale jumping robot," in *Proc. IEEE Int. Conf. Robot. Automat.*, May 2013, pp. 26–31.

[26] S. Jung, "Experiences in developing an experimental robotics course program for undergraduate education," *IEEE Trans. Educ.*, vol. 56, no. 1, pp. 129–136, Feb. 2013.

[27] S. P. Jung, "Fabrication of composite and sheet metal laminated bistable jumping mechanism," in *Proc. IEEE Int. Conf. Adv. Inf. Netw. Appl.*, 2015, pp. 48–55.

[28] M. Noh, S. W. Kim, S. An, J. S. Koh, and K. J. Cho, "Flea-inspired catapult mechanism for miniature jumping robots," *IEEE Trans. Robot.*, vol. 28, no. 5, pp. 1007–1018, Oct. 2012.

[29] Q. V. Nguyen and H. C. Park, "Design and demonstration of a locust-like jumping mechanism for small-scale robots," *J. Bionic Eng.*, vol. 9, no. 3, pp. 271–281, 2012.

[30] A. L. Desbiens, M. T. Pope, D. L. Christensen, E. W. Hawkes, and M. R. Cutkosky, "Design principles for efficient, repeated jumpgliding," *Bioinspiration Biomimetics*, vol. 9, no. 2, p. 025009, 2014.

[31] J. Zhao, N. Xi, B. Gao, M. W. Mutka, and L. Xiao, "Development of a controllable and continuous jumping robot," in *Proc. IEEE Int. Conf. Robot. Automat.*, May 2011, pp. 4614–4619.

[32] V. Zaitsev, O. Gvirsman, U. B. Hanan, A. Weiss, and G. Kosa, "A locust-inspired miniature jumping robot," *Bioinspiration Biomimetics*, vol. 10, no. 6, p. 066012, 2015.

[33] J. Zhao, W. Yan, N. Xi, M. W. Mutka, and L. Xiao "A miniature 25 grams running and jumping robot," in *Proc. IEEE Int. Conf. Robot. Automat.*, May/Jun. 2014, pp. 5115–5120.

[34] M. A. Woodward and M. Sitti, "MultiMo-Bat: A biologically inspired integrated jumping–gliding robot," *Int. J. Robot. Res.*, vol. 33, no. 12, pp. 1511–1529, 2014.

[35] S. A. Stoeter and N. Papanikolopoulos, "Autonomous stair-climbing with miniature jumping robots," *IEEE Trans. Syst., Man, Cybern. B, Cybern.*, vol. 35, no. 2, pp. 313–325, Apr. 2005.

[36] F. B. Mathis and R. Mukherjee, "Apex height control of a two-mass robot hopping on a rigid foundation," *Mechanism Mach. Theory*, vol. 105, pp. 44–57, Nov. 2016.

[37] G. He and Z. Geng, "Dynamics synthesis and control for a hopping robot with articulated leg," *Mechanism Mach. Theory*, vol. 46, no. 11, pp. 1669–1688, 2011.

YANHENG ZHANG received the B.S. degree in mechanical engineering from Shandong University, Jinan, China, in 2000, the M.S. degree in mechanical engineering from the Qingdao University of Science and Technology, Qingdao, China, in 2003, and the Ph.D. degree in mechanical engineering from Beihang University, Beijing, China, in 2007.

He is currently an Associate Professor with the Automation School, Beijing University of Posts and Telecommunications, Beijing. His research interests include spherical robot, modular manipulator, mechanism design, and pipe robot.

LUFENG ZHANG received the B.S. degree in mechanical design manufacturing and automation from the East China University of Science and Technology, Shanghai, China, in 2015, and the M.S. degree in mechanical engineering from the Beijing University of Posts and Telecommunications, Beijing, China. He is currently pursuing the Ph.D. degree with the Automation School, Beijing University of Posts and Telecommunications.

His research interests include mobile robot, jumping robot, mechanism design, and control.

WEI WANG received the B.S. degree in mechanical engineering and automation from Beihang University, Beijing, China, in 2005, and the Ph.D. degree majoring in mechanical design and theory from the Institute of Mechanical Engineering and Automation, Beihang University, in 2009.

He is currently an Assistant Professor with Beihang University. Focused on the study of variable stiffness joints applied to bionic/humanoid robots, robotic force control and application, and robot calibration and application, his research interests mainly include robotic manipulation and robotic machining.

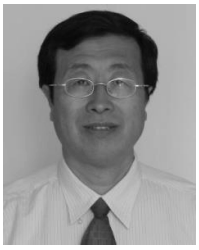

YANGMIN LI (M'98–SM'04) received the Ph.D. degree from Tianjin University, China, in 1994. He was a Lecturer with the South China University of Technology from 1994 to 1995, a fellow with the International Institute for Software Technology, United Nations University, in 1996, a Visiting Scholar with the University of Cincinnati in 1996, and a Post-Doctoral Research Associate with Purdue University, West Lafayette, IN, USA, in 1997.

He is currently a Professor with the Department of Industrial and Systems Engineering, The Hong Kong Polytechnic University. His major research includes robotics, nanotechnology, mechatronics, and control.

QINGWEN ZHANG received the B.S. degree in mechatronic engineering from East China Jiaotong University, Jiangxi, China, in 2016. He is currently pursuing the M.S. degree in mechanical engineering with the Beijing University of Posts and Telecommunications, Beijing, China.

His research interests include mobile robot, jumping robot, inspection robot, pipe robot, mechanism design, and control.